Textile & Leather Review

ISSN 2623-6281 | www.tlr-journal.com | 10.31881/TLR

Study on Parameter Optimization of Shearer Drum in Extremely Thin Seam

Jianghao Zhu

How to cite: Zhu J. Study on Parameter Optimization of Shearer Drum in Extremely Thin Seam. Textile & Leather Review. 2026; 9:2922-2940.https://doi.org/10.31881/TLR.2026.2922

How to link: https://doi.org/10.31881/TLR.2026.2922

Published: 25 April 2026

Study on Parameter Optimization of Shearer Drum in Extremely Thin Seam

Jianghao Zhu
College of Mechanical Engineering, Xi'an University of Science and Technology, Xi'an 710054, Shaanxi, China
15802900609@163.com

Article
https://doi.org/10.31881/TLR.2026.2922
Published 25 April 2026

ABSTRACT

The mechanical properties of mine roof strata affect the safety of fully mechanized mining face. The roof is easy to collapse, under the action of cutting vibration and gravity. In ultra-thin coal seams with a thickness of less than 0.8 meters and relatively high coal hardness, the cutting of coal mining machines will cause serious interference to the weak roof, thereby reducing coal quality and endangering production safety. To address this issue, this study established a cutting dynamics model of the shearer drum for ultra-thin coal seams under soft roof conditions using the discrete element method in EDEM. Based on the single factor method and using the top plate damage rate as the evaluation index, the influence of drum structure and operating parameters on soft top plate damage was systematically studied. The results show that the drum diameter is 650 mm, the hub diameter is 325 mm, the traction speed is 2 m/min, and the cutting depth is 650 mm under the single factor condition, and the shearer drum in ultra-thin coal seam has achieved the best cutting effect respectively.

KEYWORDS

extremely thin coal seam, shearer, discrete element method, roof damage

INTRODUCTION

Coal is the most abundant energy resource in China, accounting for 94% of the country's identified fossil energy reserves, and it constitutes an essential foundation for the sustainable development of the national economy [1]. In 2023, coal consumption accounted for 55.3% of China's total energy consumption. From the perspective of the national energy consumption structure in recent years, coal has remained the primary energy source and continues to occupy a dominant position in the energy mix [2], serving as a stabilizer and cornerstone of China's energy security [3]. Thin coal seam resources in China are widely distributed and abundant in reserve [4], with recoverable reserves of approximately 6.5 billion tons. Thin or ultra-thin coal

seams are present in more than 400 producing mines across nearly 80 mining areas nationwide [5], accounting for over 20% of the total recoverable reserves [6]. In recent years, with the gradual depletion of readily extractable thick and medium-thick coal seams, the exploitation of thin coal seams has become an inevitable choice [7].

In some mining areas, ultra-thin coal seams are characterized by relatively hard coal and soft-rock roofs. Owing to the mismatch between shearer drum parameters and geological conditions, the weak roof undergoes extensive collapse under the disturbance induced by cutting impact and vibration. Part of the fallen roof accumulates on the shearer body, thereby increasing the machine load and impairing heat dissipation, which poses significant safety hazards. In addition, the collapsed gangue becomes mixed with the coal, reducing coal quality and adversely affecting the economic benefits of mining operations. At present, numerous studies have investigated the relationship between drum parameters and the failure of hard coal seams and soft roof strata. Bo Y. et al. [8] demonstrated through simulation that shear failure exerts the greatest influence on roof frag mentation during drum cutting. Ji Guoqiang et al. [9] simulated the entire drum cutting process and analyzed the variation in rock stress. Tian Zhen et al. [10] established a roof model based on the Drucker–Prager yield criterion and obtained the force distribution within the roof as well as the variation law of drum loading. Ghamgosar M. [11] explored the differences in rock crack evolution under cyclic and static loading, revealing that the final failure of rock results from the coalescence of numerous tensile cracks oriented parallel or oblique to the loading direction. Zhao Fujun [12], using ANSYS software, simulated the failure process of granite under combined dynamic and static loading, and showed the influence of dynamic loading on the crack propagation area of granite under coupled loading conditions.

The above research mainly focuses on the fracture characteristics and evolution behavior of mechanical properties of coal rock materials under different physical conditions, aiming to improve the cutting efficiency of coal mining machine drums on coal walls, and clarify the evolution and prevention mechanism of roof fracture. However, there are few studies reporting the damage patterns of low hardness and low strength roof under different drum shaped parameter combinations in ultra-thin coal seam conditions. In this paper, the drum of MG200/468-WD ultra-thin coal seam shearer is taken as the research object, and the drum cutting dynamics is established based on the discrete element theory, and the influence of each drum parameter on the roof is analyzed.

THEORETICAL ANALYSIS OF ROOF DAMAGE INDUCED BY SHEARER DRUM CUTTING IN ULTRA-THIN COAL SEAMS

The Mechanical Parameters of Roof Materials

The occurrence characteristics of coal seams are governed by the coupled effects of their depositional evolutionary history and subsequent tectonic modification. The structure of coal can be classified into primary structures and secondary structures induced by tectonic stress fields. The mechanical behavior of roof is closely associated with their multiscale structural characteristics. In particular, key parameters, including compressive strength, shear modulus, and hardness coefficient, directly determine the deformation and failure modes of the roof under mining-induced stress fields.

The relationships among the compressive strength σ_y , shear strength σ_j , and tensile strength σ_l can be approximately expressed as follows:

$$\sigma_y : \sigma_j : \sigma_l = (0.1 \sim 0.4) : (0.03 \sim 0.1) \tag{1}$$

Considering the distribution characteristics of the roof contact interface, the surface strength can be calculated as:

$$P_K = \frac{1}{A_e}(\sum_{i=1}^{n} \frac{F_i^m}{V_0})\frac{1}{m} \tag{2}$$

where P_K is the contact strength of the roof, in MPa; F_i is the contact force measured in the *i*-th test, in N; A_e is the effective contact area, in mm ^{2} ; *m* is the Weibull modulus; and V_0 is the reference volume.

The failure resistance of the roof can be quantitatively characterized by the Protodyakonov firmness coefficient *f*, which comprehensively reflects both the strength and structural integrity of the roof, as shown in Table 1.

Table 1. Classification of the firmness of roof

Type of roof	Lignite	Mudstone	Argillaceous siltstone	Fine sandstone
Firmness coefficient f	0.6~1.0	1.2~2.0	3.5~5.0	4.5~7.0

During the mining of ultra-thin coal seams, the mechanical properties of roof are key factors affecting both the cutting efficiency of the shearer and the stability of the roof. The compressive strength of roof materials

directly determines their failure characteristics and energy dissipation behavior under mining-induced stresses. Moreover, significant differences exist in the compressive strength of different roof lithologies, such as mudstone and siltstone. The corresponding compressive strength values are listed in Table 2.

Table 2. Compressive strength of roof

Classification of roof	Lignite	Mudstone	Argillaceous siltstone	Fine sandstone
Compressive strength σ /MPa	6~9	21~77	24~65	48~112

Damage Mechanism of Soft Roof under Cutting Disturbance

The pick is a key tool for cutting coal seams and fragmenting rock in coal mining and is widely used in mechanical equipment such as shearers and road-headers. It is characterized by high cutting efficiency, strong adaptability, and good wear resistance, enabling long-term stable operation under complex mining conditions. During the cutting process, the resistance acting on the pick exhibits dynamic variation, which is mainly attributed to differences in the mechanical properties of the and changes in the number of picks simultaneously involved in cutting. The forces exerted on the pick by the roof include cutting resistance Z_j, traction resistance Y_j, and lateral force X_j [13,14], as shown in Fig. 1.

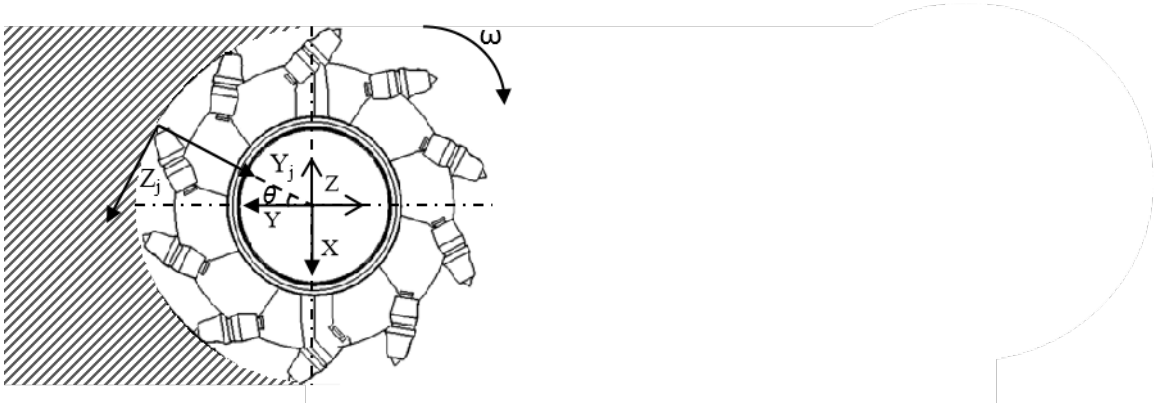

Figure 1. Schematic diagram of the forces acting on the pick during cutting

$$\{Z_j = \overline{A}\frac{1.75d+3}{0.5d+K_\psi h^{0.5}}h \times s \times K_\eta \times K_\alpha \times K_\beta \times K_c \times K_{ot} \times \frac{1}{\cos\theta}$$

$$Y_j = (0.5-0.8)Z_j \tag{3}$$

$$X_j = Z_j(\frac{1.4\times10^{-3}}{0.1h+0.3\times10^{-3}}+0.5)\frac{h}{s}$$

where $\overline{A}$ is the average cutting resistance, in N/mm; *d* is the pick diameter, in mm; *h* is the maximum cutting depth of the pick, in mm; *s* is the cutting line spacing between adjacent vanes, in mm; K_ψ is the brittleness coefficient; K_η is the influence coefficient of the free surface; K_α is the structural coefficient of the rake face of the pick; K_β is the influence coefficient of the pick angle; K_c is the influence coefficient of the pick arrangement; θ is the installation angle of the pick, in °; and K_{ot} is the ground pressure influence coefficient. During the cutting process of cohesive coal, the rotation of the helical drum induces dynamic evolution in the mechanical response. The number of picks involved in cutting and their spatial distribution vary continuously, causing the three-dimensional resistance components, including cutting resistance, traction resistance, and lateral resistance, to exhibit pronounced time-dependent characteristics. The corresponding force calculation equations are given as follows:

$$\begin{aligned} F_x &= \sum_{i=1}^{m} F_{xi} = \sum_{i=1}^{m} X_i \\ F_y &= \sum_{i=1}^{m} F_{yi} = -\sum_{i=1}^{m} (y_i \sin\theta_i + z_i \cos\theta_i) \\ F_z &= \sum_{i=1}^{m} F_{zi} = \sum_{i=1}^{m} (z_i \sin\theta_i + y_i \cos\theta_i) \end{aligned} \tag{4}$$

where *m* is the number of picks involved in cutting; F_x is the resultant force acting on the drum along the X-axis, in N; F_y is the resultant force acting on the drum along the Y-axis, in N; F_z is the resultant force acting on the drum along the Z-axis, in N; and θ_i is the positional angle of the *i*-th pick relative to the drum, in rad. Under ultra-thin coal seam conditions, the normal force acting on the pick, which is perpendicular to the pick surface, and the tangential force, which is parallel to the pick surface, are transmitted to the drum through the pick body. The corresponding stress calculation equations are given as follows. When the normal stress of the roof, σ_{n} , exceeds the interlayer bonding strength, σ_{b} , tensile failure occurs:

$$\sigma_{\mathrm{n}} = \frac{\sum \mathbf{Z_i} \sin \boldsymbol{\varphi_i} + \sum \mathbf{Y_i} \cos \boldsymbol{\varphi_i}}{A_{\mathbf{e}}} \tag{5}$$

where $A_{\mathbf{e}}$ is the cutting area of the drum, given by $A_{\mathbf{e}} = \pi(D_{\mathbf{c}}^2 - H^2)/4$; and $\varphi_{\mathbf{i}}$ is the contact angle between the *i*-th pick and the roof.

The tangential force of the pick is transmitted to the weak interlayer plane of the roof through fragmentation. When the tangential stress of the roof, τ , exceeds the interlayer bonding strength, $\tau_{\mathbf{b}}$, shear slip is induced:

$$\tau = \frac{\sum Y_i \sin \phi_i}{A_s} \geq \tau_b \tag{6}$$

where $A_{\mathbf{s}}$ is the shear area, with $A_{\mathbf{s}} = L \cdot t$; L is the roof length; t is the roof thickness; and $\phi_{\mathbf{i}}$ is the angle between the traction resistance of the *i*-th pick and the weak interlayer plane.

As indicated by the above equations, the mechanical failure of the roof exhibits a complex functional relationship with drum diameter, hub diameter, and helix angle. Therefore, in this study, the degree of roof damage is adopted as the evaluation index, while drum diameter, hub diameter, helix angle, haulage speed, and cutting depth are selected as the influencing factors to reveal their effects on roof failure and to optimize the parameters of the shearer drum. The MG200/468-WD shearer drum for ultra-thin coal seams is taken as the research object. This shearer adopts a mining mode in which the front drum cuts the floor and the rear drum cuts the roof. The main drum parameters are as follows: drum diameter, 750 mm; hub diameter, 375 mm; helix angle, 14°; vane diameter, 650 mm; and number of vanes, 2.

Particle Parameter Setting and Establishment of the Coal Wall Model

To ensure that the simulation model more closely reflects actual working conditions while maintaining computational efficiency, the model parameters and material parameters were defined in the preprocessing interface of EDEM. According to the geological report of a coal mine in Shaanxi Province, the roof lithologies include mudstone and argillaceous siltstone, with fine sandstone being the predominant roof rock type. In the EDEM pre-processing module, the material properties required for the simulation were created, as listed in Table 3.

Table 3. Physical parameters of roof particles

Material	Poisson's ratio	Density/kg·m^{-3}	Shear modulus/Pa
Coal	0.28	1280	2.01×10^9
Mudstone	0.19	2555	1.60×10^{10}
Argillaceous siltstone	0.24	2618	3.82×10^9
Fine sandstone	0.21	2700	6.27×10^9
Drum	0.31	7800	8.10×10^{10}

In the Materials interface of the EDEM pre-processing module, the model parameters and material parameters were defined. The contact parameters of the roof particles are listed in Table 4.

Table 4. Contact parameters of roof particles

Contact pair	Coefficient of restitution	Static friction coefficient	Dynamic friction coefficient
Coal–coal	0.10	0.65	0.10
Coal–drum	0.35	0.85	0.65
Coal–mudstone	0.17	0.55	0.40
Coal–argillaceous siltstone	0.15	0.55	0.35
Coal–sandstone	0.50	0.50	0.41
Mudstone–mudstone	0.13	0.50	0.43
Mudstone–drum	0.50	0.50	0.01
Argillaceous siltstone–argillaceous siltstone	0.10	0.50	0.43
Argillaceous siltstone–drum	0.50	0.50	0.01
Fine sandstone–fine sandstone	0.50	0.50	0.41
Fine sandstone–drum	0.50	0.60	0.70

According to the operating conditions of a coal mine in Shaanxi Province, the cutting depth was set to 800 mm, the drum haulage speed to 3 m/min, and the rotational speed to 75 r/min, as illustrated in Fig. 2.

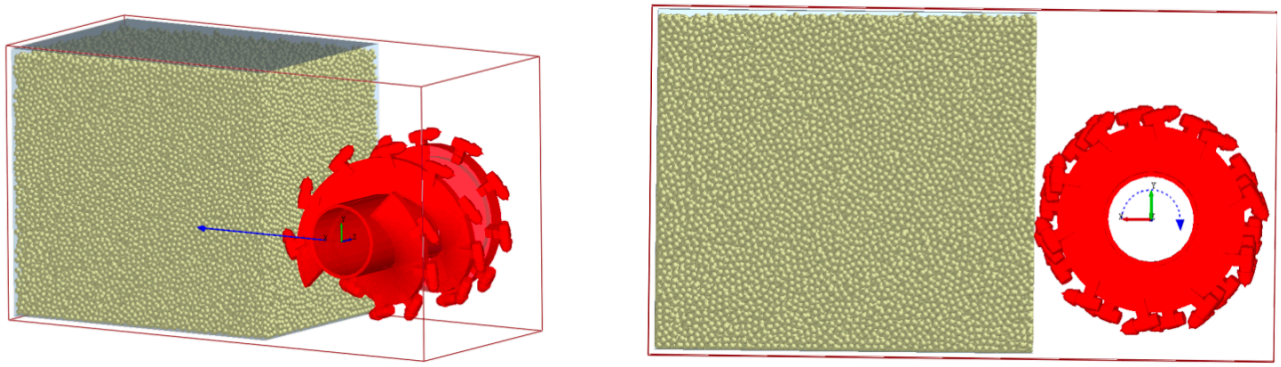

Figure 2. Motion parameter settings

The initial parameters were defined, and to ensure simulation accuracy, the time step was set to 20%, with a total simulation time of 18.5 s. The total number of roof bonding bonds and interlayer bonding bonds was statistically analyzed. The cutting dynamics model and a schematic of the bonds are shown in Fig. 3. Based on the simulation results, the bond breakage ratio of the roof was adopted as the evaluation index to determine the damage rate of the roof induced by the drum.

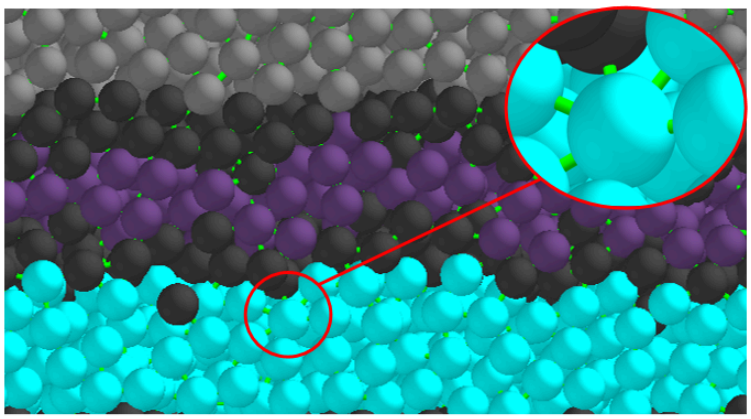

Figure 3. Schematic diagram of roof bond bonds

$$\xi = \frac{\sum M_1}{\sum M_2} \tag{7}$$

where ξ is the roof damage rate; $\sum M_1$ is the total number of roof bonds before cutting; and $\sum M_2$ is the total number of roof bonds after cutting.

A parametric three-dimensional model of the MG200/468-WD shearer drum for ultra-thin coal seams was established using SolidWorks. The resulting three-dimensional model was then imported into EDEM to construct a discrete element dynamic model of the shearer drum cutting process, as shown in Fig. 4.

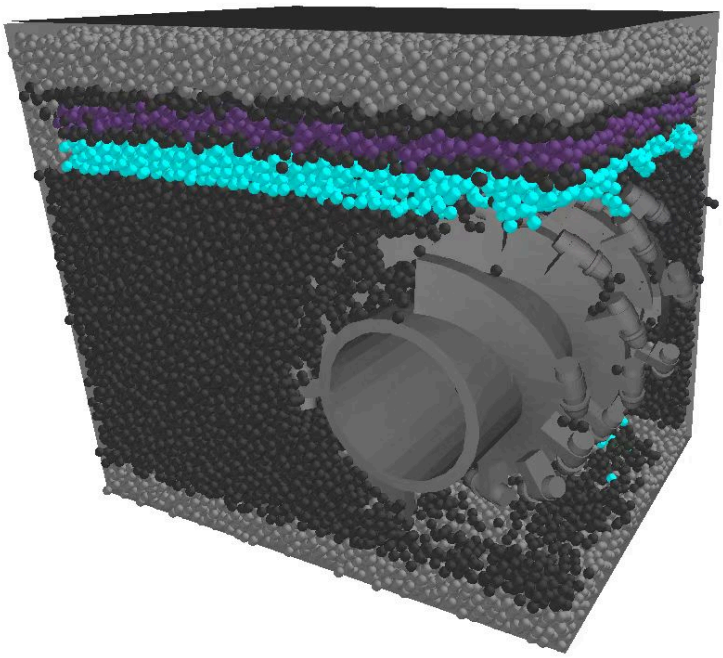

Figure 4. Drum cutting simulation model

SIMULATION ANALYSIS OF THE DRUM CUTTING PROCESS

The principal factors affecting roof damage include drum diameter, hub diameter, helix angle, haulage speed, rotational speed, and cutting depth. A single-factor parametric analysis was conducted to investigate the influence of each parameter on roof damage and to optimize roof stability. The initial drum parameters were set as follows: drum diameter, 750 mm; hub diameter, 375 mm; helix angle, 14°; haulage speed, 3 m/s; rotational speed, 85 r/min; and cutting depth, 800 mm.

Simulation Study on the Effect of Drum Diameter on Roof Damage Rate

Different drum diameters exert a significant influence on the disturbance and damage of the roof. In this study, single-factor tests were independently carried out for drums with diameters of 650, 700, 750, and 800 mm, while all other variables were kept constant. By calculating the roof damage rate under each drum diameter, the influence law of drum diameter on roof damage was obtained, as shown in Fig. 5.

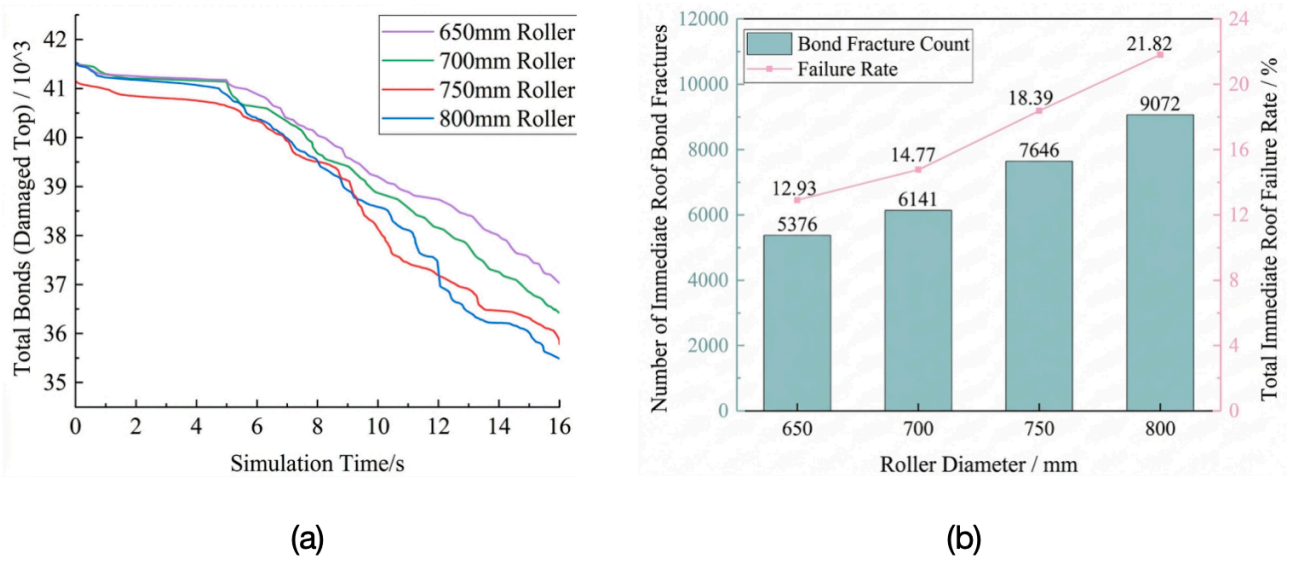

Figure 5. Influence of different drum diameters on roof damage: (a) Variation trend of the number of roof bonds; (b) Number of broken roof bonds and damage rate

As shown in Fig. 5（a）, the total number of roof bonds began to decrease significantly after 4 s. The roof damage rate increased with increasing drum diameter. Among the tested cases, the 800 mm drum produced the largest number of broken roof bond bonds, with a roof damage rate of 21.82%.

The influence of different drum diameters on the interlayer damage rate of the roof is also illustrated in Fig. 5（b）. The larger drums, with diameters of 800 and 750 mm, caused more pronounced damage at

the coal–mudstone interface, with interlayer damage rates of 21.13%and 20.87%, respectively, whereas the corresponding values for the smaller 700 and 650 mm drums were only 11.79% and 9.51%. The 800 mm drum also produced substantially greater damage at the coal–argillaceous siltstone interface than the other drums, reaching 14.68%, while the other three drums caused relatively limited damage. For the coal–fine sandstone interface, the larger-diameter drums produced comparable levels of damage, whereas the 650 mm drum caused significantly less damage to the roof, with a value of only 11.71% (Figure 6).

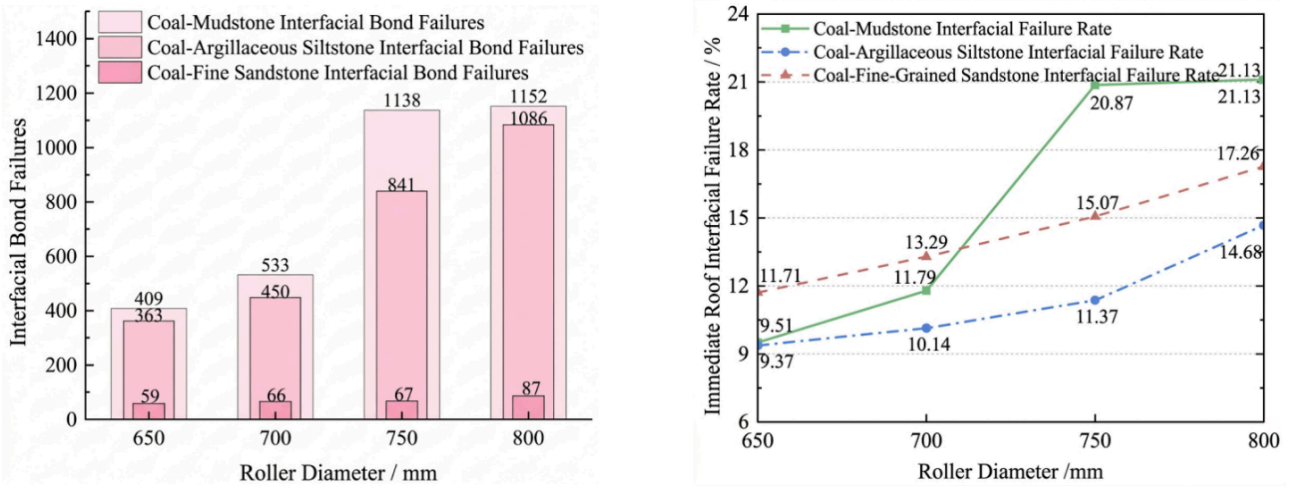

Figure 6. Influence of different drum diameters on the interlayer damage rate of the roof

Compared with smaller-diameter drums, the 800 mm drum provides a larger contact area with the particles, causing the bond bonds to bear greater stress and thereby increasing the probability of bond breakage. In addition, a larger drum diameter induces more intense vibration, making the forces acting on the particles more complex and non-uniform. This results in stronger disturbance during particle flow and further promotes the fatigue failure of the bond bonds.

Simulation Study on the Effect of Hub Diameter on Roof Damage Rate

In this study, single-factor tests were independently conducted for hub diameters of 325, 350, 375, and 400 mm, while all other variables were kept constant. By calculating the roof damage rate under each hub diameter, the influence law of hub diameter on roof damage was obtained, as shown in Fig. 7.

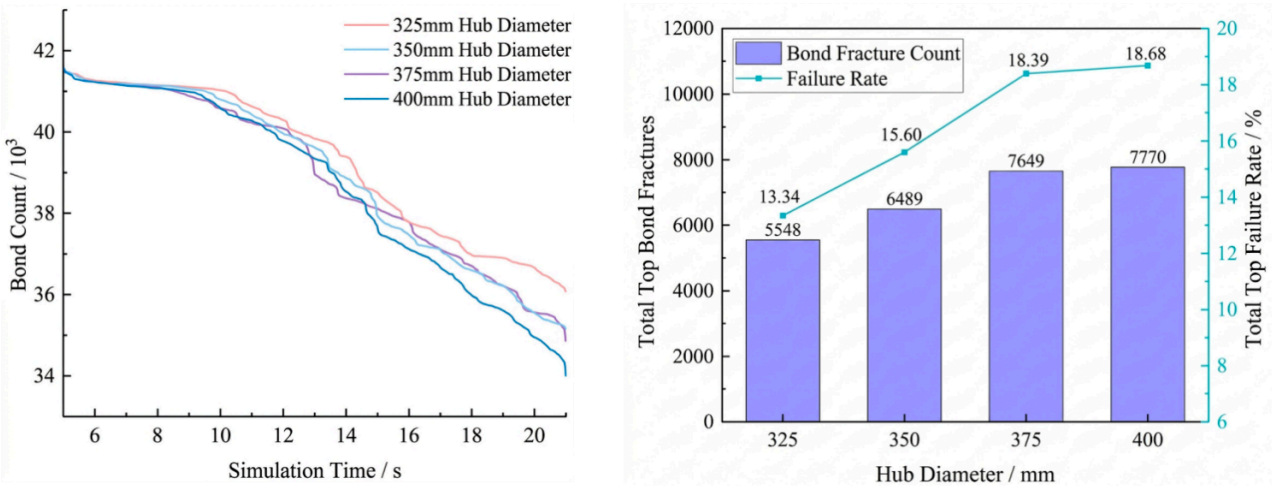

Figure 7. Influence of different hub diameters on roof damage

As shown in Fig. 7, with increasing hub diameter, the number of roof bond bonds decreased accordingly. The highest roof damage rate was obtained at a hub diameter of 400 mm, reaching 18.68%, while the value corresponding to a hub diameter of 375 mm was comparable, at 18.39%.

The influence of different hub diameters on the interlayer damage rate of the roof is presented in Fig. 8. The drum with a hub diameter of 400 mm caused the most severe damage at the coal–mudstone interface, with an interlayer damage rate of 20.43%, whereas the drum with a hub diameter of 325 mm produced an interlayer damage rate of only 16.14%. The curves for the interlayer damage rates at the coal–argillaceous siltstone and coal–fine sandstone interfaces further indicate that drums with larger hub diameters consistently caused more severe roof damage than those with smaller hub diameters.

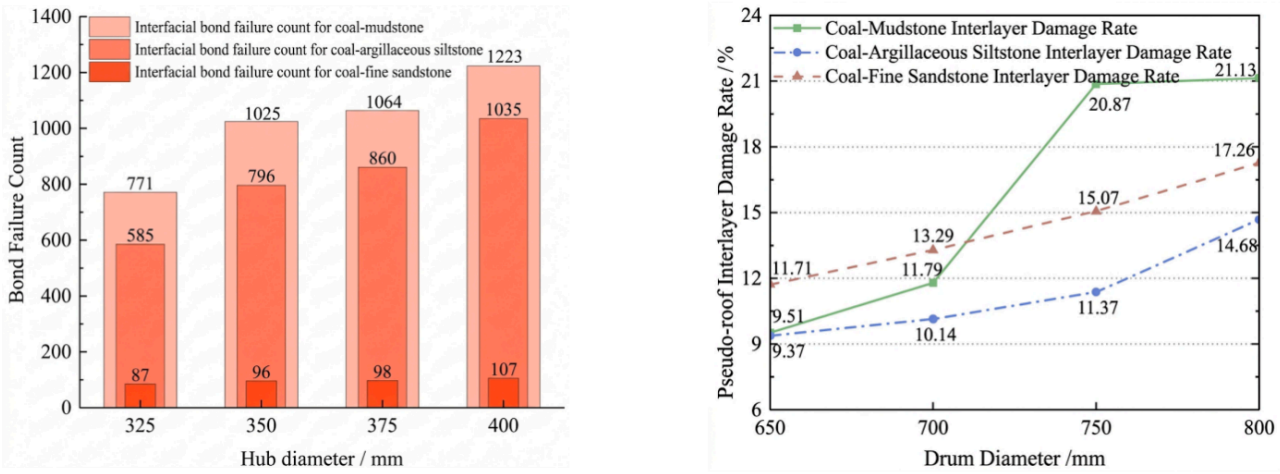

Figure 8. Influence of different hub diameters on the interlayer damage rate of the roof

Figure 9 presents the average contact force of the roof bonds. The normal force mainly reflects the compressive and supporting interactions between particles. As the hub diameter increases, the normal contact force acting on the bonded contacts also increases, leading to local stress concentration and consequently aggravating roof damage.

The tangential force mainly reflects the frictional and shear interactions between particles. Owing to the stratified structure of the roof, which is characterized by relatively low shear strength and bonding strength, a larger hub diameter intensifies the shear interaction with the roof. The increase in tangential force generates greater shear stress within weak interlayers, thereby exacerbating the shear failure of the roof.

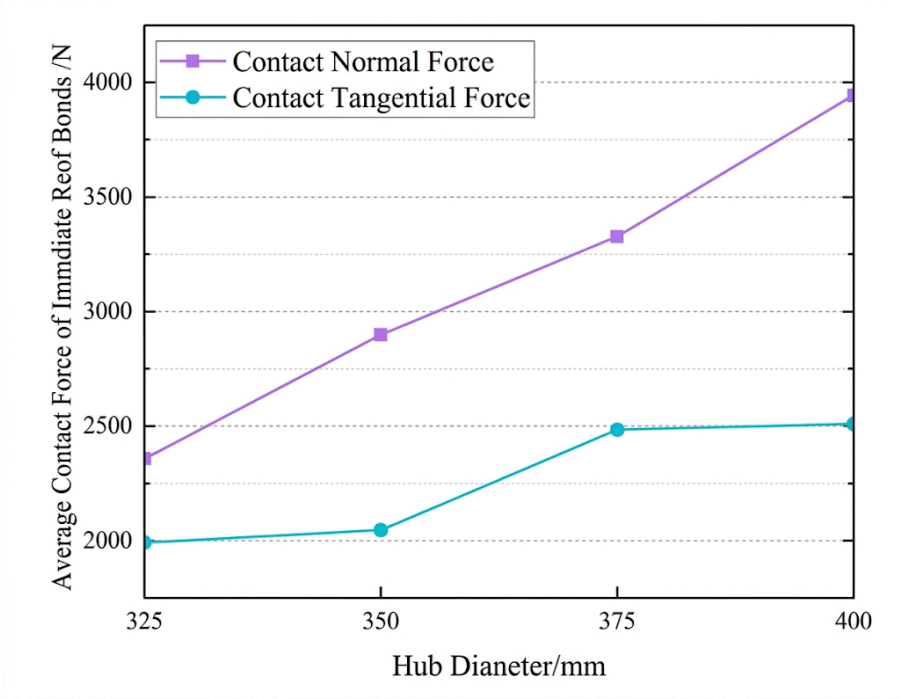

Figure 9. Average contact force of roof bonds

Simulation Study on the Effect of Helix Angle on Roof Damage Rate

In this study, single-factor tests were independently conducted for helix angles of 12°, 14°, 16°, and 18°, while all other variables were kept constant. By calculating the roof damage rate under each helix angle, the influence law of helix angle on roof damage was obtained, as shown in Fig. 10.

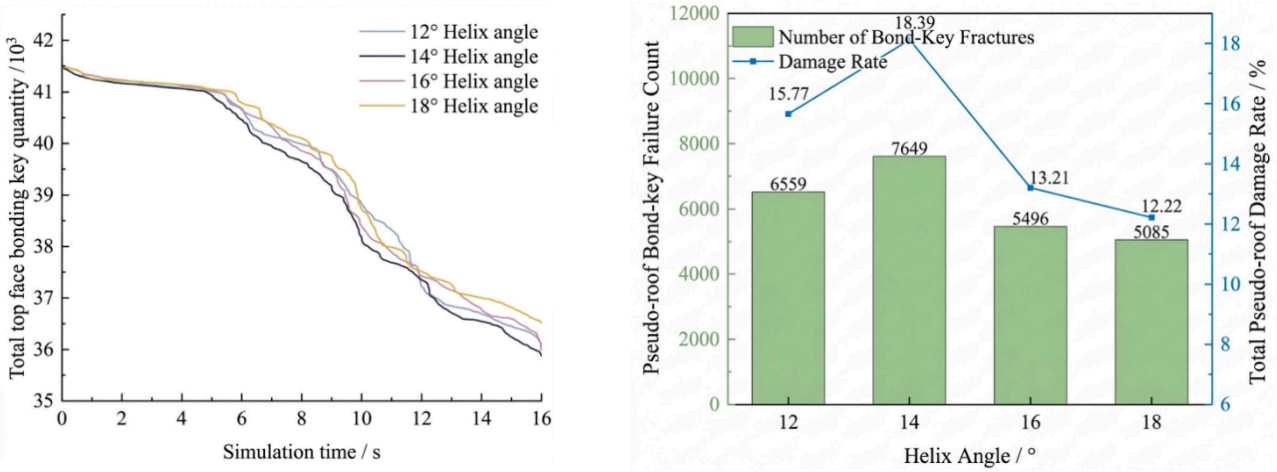

Figure 10. Influence of different helix angles on roof damage

As shown in Fig. 10, with increasing helix angle, the roof damage rate first increased and then decreased, reaching its maximum value of 18.39% at a helix angle of 14°. The influence of different helix angles on the interlayer damage rate of the roof is illustrated in Fig. 11. A significant negative correlation can be observed between helix angle and the interlayer damage rate of the roof. The drum with a helix angle of 14° caused the most severe damage at the coal–mudstone interface, with a damage rate of 19.74%, whereas the drums with helix angles of 16° and 18° produced relatively similar roof damage rates, at 16.78% and 16.67%, respectively.

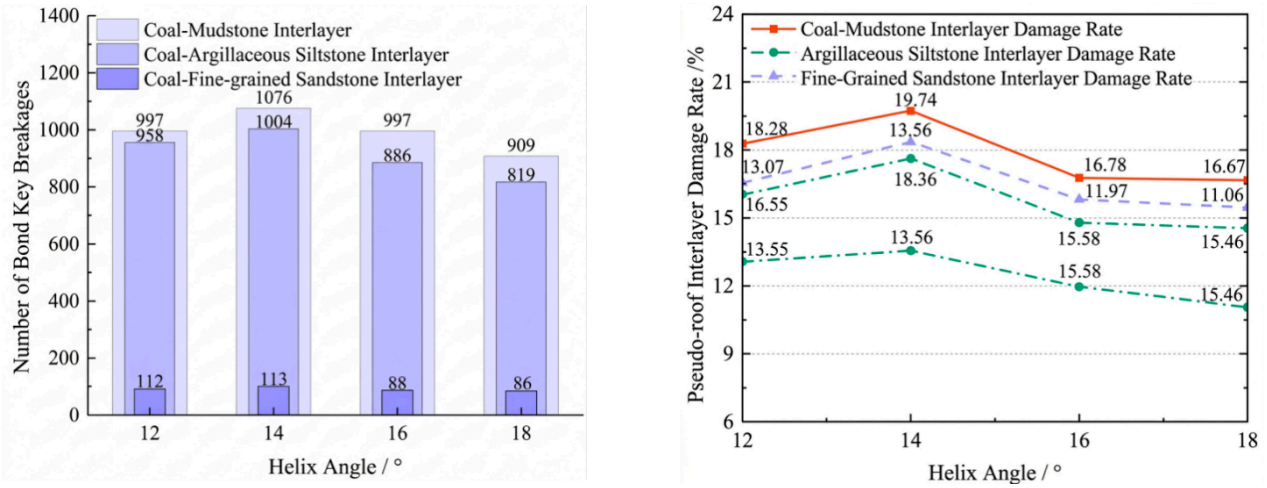

Figure 11. Influence of different helix-angle drums on the interlayer damage rate of the roof

Simulation Study on the Effect of Haulage Speed on Roof Damage Rate

In this study, single-factor tests were conducted under haulage speeds of 2, 3, 4, and 5 m/min, while all other variables were kept constant. By statistically analyzing the number of roof bond bonds and calculating the corresponding roof damage rate for each drum, the influence law of haulage speed on roof damage was obtained, as shown in Fig. 12.

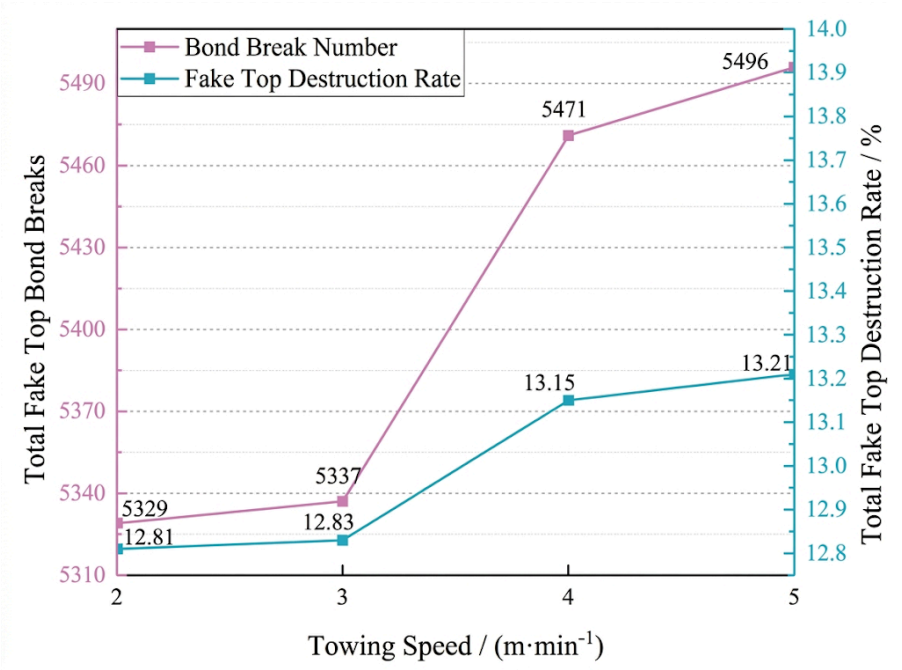

Figure 12. Roof damage rate under different haulage speeds

As shown in Fig. 12, when the haulage speed was relatively low, the disturbance induced by the drum to the roof was limited. At a haulage speed of 2 m/min, the roof damage rate was only 12.81%. With increasing haulage speed, the roof damage rate increased accordingly and reached its maximum value of 13.21% at 5 m/min.

The number of broken interlayer bond bonds and the corresponding damage rates are presented in Fig. 13. For the coal–mudstone interface, the damage rate changed only slightly as the haulage speed increased from 2 to 5 m/min, rising marginally from 23.15% to 23.92%. In contrast, the damage rate of the coal–argillaceous siltstone interface exhibited a more pronounced upward trend, increasing continuously from 10.52% at 2 m/min to 15.78% at 5 m/min. For the coal–fine sandstone interface, the damage rate increased from 19.15% to 20.32% as the haulage speed rose from 2 to 4 m/min, and then increased slightly further to 20.41% when the haulage speed reached 5 m/min.

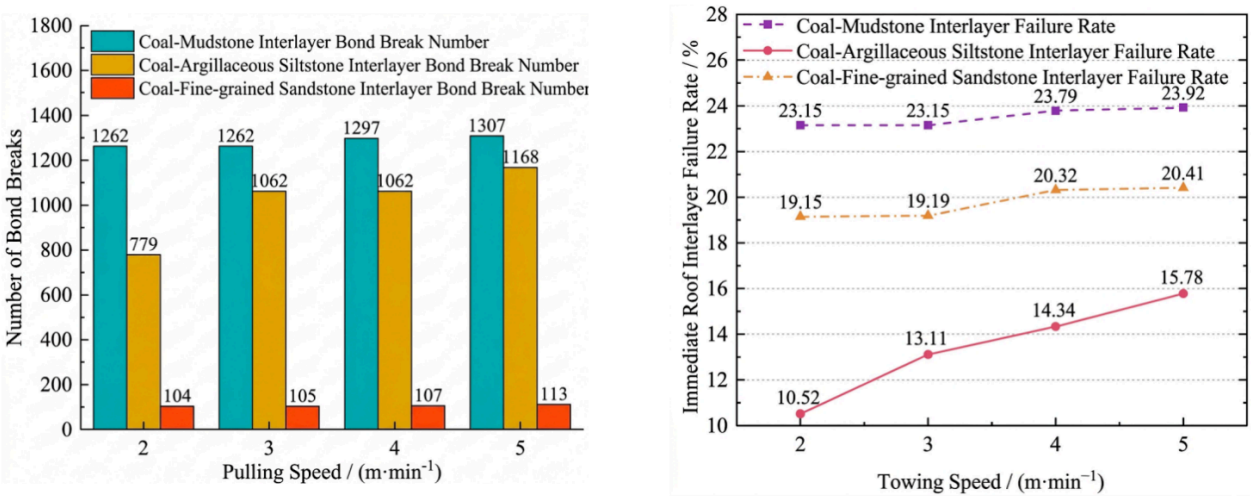

Figure 13. Broken interlayer bonds and damage rate at different haulage speeds

Under high-speed haulage conditions (5 m/min), the discharge rate of roof particles is accelerated; however, incompletely fragmented large particles accumulate within the drum and interact with newly cut coal and rock, thereby causing secondary impacts. At a lower haulage speed (2 m/min), the residence time of roof particles is prolonged, but fragmentation becomes more sufficient, which reduces impact-induced damage to the roof. Mechanical analysis further indicates that, at a low haulage speed of 2 m/min, the contact duration between the picks and the roof is longer, allowing stress to be transmitted more gradually through the force-chain network and resulting in a more uniform stress distribution within the roof region. In contrast, under high-speed conditions (5 m/min), instantaneous impacts lead to localized stress concentration and higher peak normal stress.

Figure 14 shows the average contact force of roof bond bonds under different haulage speeds. Under low-speed conditions (2–3 m/min), the ratio of tangential force to normal force is relatively high, indicating that the tangential force is significantly greater than the normal force. Owing to the longer pick–roof contact time at low speed, stress transfer is more uniform; nevertheless, the sustained action of tangential force promotes the propagation of fatigue cracks, and roof failure is dominated by shear stress, causing particle shear slip along bedding planes and shear breakage of bond bonds. Under medium- to high-speed conditions (4–5 m/min), the ratio of tangential force to normal force decreases, and the normal force becomes comparable to the tangential force, indicating that the contribution of compressive stress increases and that the failure mode shifts from shear-dominated failure to a combined compression–shear mode. Under high-speed operating

conditions, dynamic impact induces localized stress concentration and fatigue accumulation, leading to the highest bond breakage rate at 5 m/min.

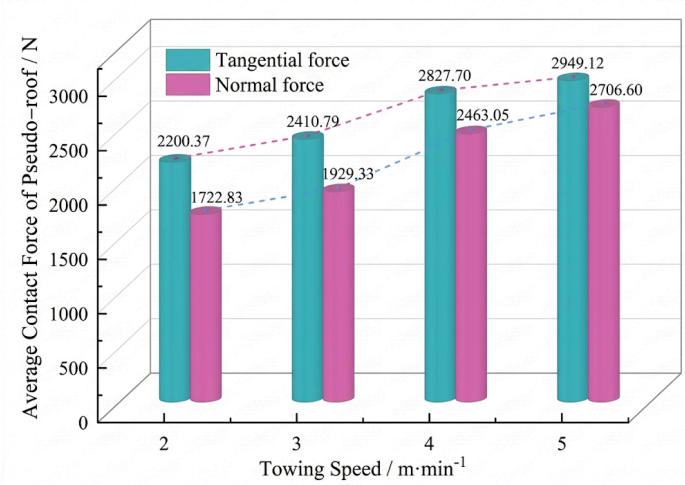

Figure 14. Average contact force of roof bonds

Simulation Study on the Effect of Cutting Depth on Roof Damage Rate

In this study, single-factor tests were conducted under cutting depths of 650, 700, 750, and 800 mm, while all other variables were kept constant. By statistically analyzing the number of roof bond bonds and calculating the corresponding roof damage rate for each drum, the influence law of cutting depth on roof damage was obtained, as shown in Fig. 15. The number of broken interlayer bond bonds and the corresponding damage rates are presented in Fig. 16.

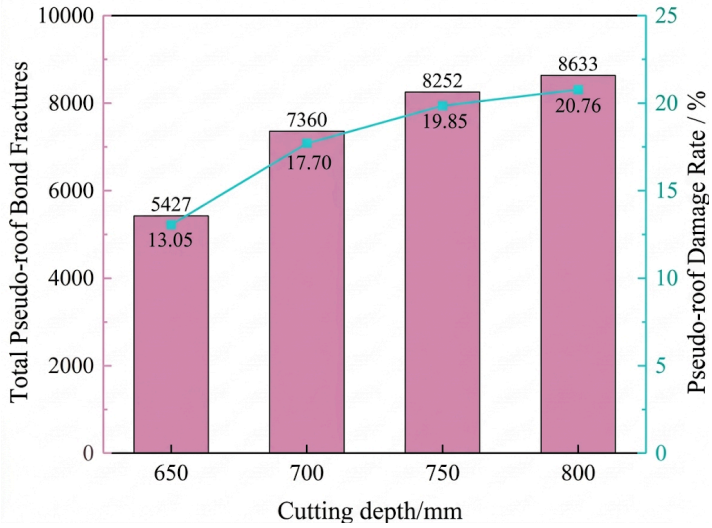

Figure 15. Total number of broken roof bonds and damage rate at different cutting depths

As shown in Fig. 15, as the cutting depth increased from 650 mm to 800 mm, the total number of broken roof bonds rose from 5427 to 8633, while the roof damage rate increased from 13.05% to 20.76%, both exhibiting an overall upward trend. When the cutting depth increased from 650 mm to 700 mm, the total number of broken roof bonds increased by 1933, and the damage rate increased by 4.65%. As the cutting depth further increased from 700 mm to 750 mm, the total number of broken bonds increased by 892, and the damage rate increased by 2.15%. When the cutting depth increased from 750 mm to 800 mm, the total number of broken bonds increased by 381, and the damage rate increased by 0.91%. These results indicate that an increase in cutting depth significantly aggravates roof damage.

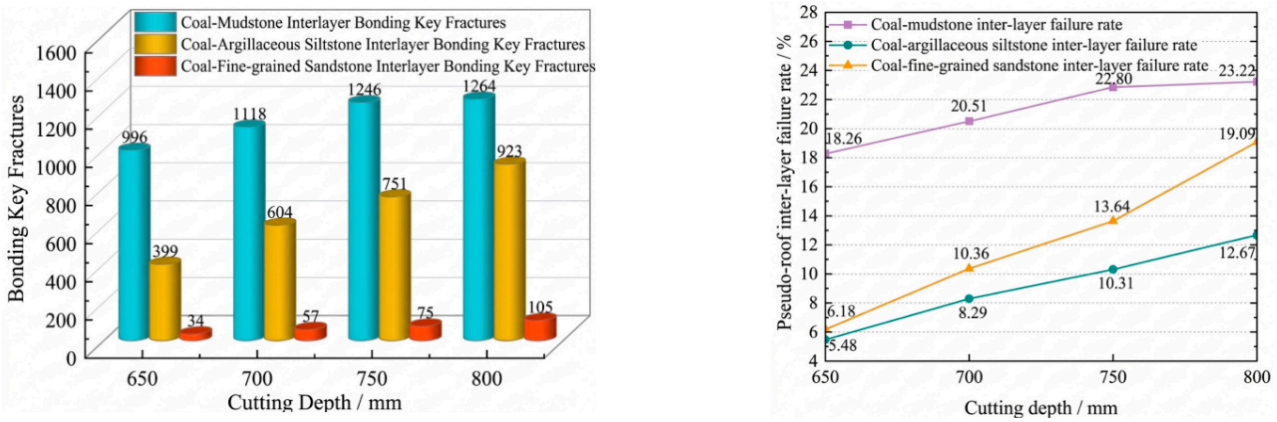

Figure 16. Broken interlayer bonds and roof interlayer damage rate at different cutting depths

As shown in Fig. 16, under low cutting-depth conditions, the disturbance induced by drum cutting on the interlayers of the roof is relatively limited. Changes in cutting depth have the most pronounced effect on damage at the coal–mudstone interface, whereas their influence on the other interlayer interfaces is comparatively smaller. At a cutting depth of 650 mm, the damage rates at the coal–argillaceous siltstone and coal–fine sandstone interfaces were only 5.48% and 6.18%, respectively. With increasing cutting depth, the damage rate increased accordingly and reached its maximum value at a cutting depth of 800 mm.

CONCLUSIONS

Taking the MG200/468-WD shearer for ultra-thin coal seams as the research object, a three-dimensional model was established in SolidWorks, and a dynamic disturbance simulation model of drum cutting under hard-coal and soft-rock roof conditions was developed in EDEM. By statistically analyzing the total number of roof bonds, the number of bonds at different interlayers, and their stress distributions, the influence laws

of the structural and operating parameters of the shearer drum on roof damage were obtained. Specifically, larger drum diameter and hub diameter led to higher roof damage rates. The minimum roof damage rates were achieved at a drum diameter of 650 mm and a hub diameter of 325 mm, with values of 12.93% and 13.44%, respectively. With increasing helix angle, the roof damage rate first increased, then decreased, and then increased again, reaching a minimum value of 12.22% at 18°. The roof damage rate also increased with increasing haulage speed and cutting depth, and the minimum values were obtained at a haulage speed of 2 m/min and a cutting depth of 650 mm, at 12.81% and 13.05%, respectively. Roof damage induced by haulage speed was dominated by tangential-force-related failure, whereas damage caused by cutting depth was primarily characterized by compressive failure.

Author Contributions

Methodology and writing are all done by Jianghao Zhu. All authors have read and agreed to the published version of the manuscript.

Conflicts of Interest

The author declares no conflict of interest.

Funding

This research received no external funding.

Acknowledgement

Not applicable.

REFERENCES

[1] Liu F, Cao WJ, Zhang JM, Cao GM, Guo LF. Current technological innovation and development direction of the 14thFive-Year Plan period in China coal industry. Journal Of China Coal Society. 2021; 46(1): 1-15. doi: 10.13225/j.cnki.jccs.2021.0042

[2] Yuan L, Zhang T, Wang YH, Wang XZ, Wang YT, Hao XJ. Scientific problems and key technologies for safe and efficient mining of deep coal resources. Journal Of China Coal Society. 2025; 50(1): 1-12. doi: 10.13225/j.cnki.jccs.YG25.0016

[3] Zhang L, Wang G, Liu ZG, et al. Research of the present situation and development trend of intelligent coal mine construction market. Coal Science and Technology. 2024; 52(11): 29-44. doi: 10.12438/cst.2024-0690

[4] Wang Gf, Ren HW, Fu JX. Challenge and path of high-quality development of coal mine intelligent construction. Coal Science and Technology. 2025; 53(1): 1-18. doi: 10.12438/cst.2024-1787

[5] Zhai YS, Shi CX, Lv X, Guo D. Development status and key technologies of thincoal seam drum shearer. Coal Engineering. 2020; 52(7): 182-186. doi: 10.11799/ce202007038

[6] Kang ZP, Luo Y, Ren B, Duan CR, Xiao DC. Study on surrounding rock failure characteristics and control technology of gob-side entry retaining in “three hard” thin coal seam. Journal Of Mining Science And Technology. 2024; 9(3): 446-454. doi: 10.19606/j.cnki.jmst.2024.03.013

[7] Yuan Y, Tu SH, Chen ZS, Zhang C, Wang Chen. Current situation and development of intelligent mining technology forthin coal seams. Coal Science and Technology. 2020; 48(5): 1-17. doi: 10.13199/j.cnki.cst.2020.05.001

[8] Lv X, Chen F, Zhang J. Numerical simulation study on multiphase flow pattern of hydrate slurry. Petroleum Science. 2023; 20(06): 3897-3917. doi: 10.1016/j.petsci.2023.08.008

[9] Ji GQ, Lian ZS, Lu C. The Cutting Force Simulation of Conical Bits Based on LS-DYNA. Friend of Science Amateurs (B Edition). 2008; (4): 131-132. doi: 10.13436/j.mkjx.2009.03.011

[10] Tian Z, Zhao LJ, Zhang JJ. Study on Mechanical Behaviour of Spiral Drum under Complex Condition of Coal Seam. Mechanical Science and Technology for Aerospace Engineering. 2019; 38(7): 1041-1047. doi: 10.13433/j.cnki.1003-8728.2019.20180283

[11] Ghamgosar M, Erarslan N, Williams DJ. Experimental investigation of fracture process zone in rocks damaged under cyclic loadings. Experimental mechanics. 2017; 57: 97-113. doi: 10.1007/s11340-016-0216-4

[12] Farhoumand A, Ebrahimi R. Experimental investigation and numerical simulation of plastic flow behavior during forward-backward-radial extrusion process. Progress in Natural Science: Materials International. 2016; 26(06): 650-656. doi: 10.1016/j.pnsc.2016.12.005

[13] Zhao LJ, Ma YZ. Reliability research on shearer cutting unit based on multi-body dynamics. Journal Of China Coal Society. 2009; 34(9): 1271-1275. doi: 10.13225/j.cnki.jccs.2009.09.015

[14] Zhao LJ, Dong MM. Load problems of working mechanism of the shearer in containing pyrites and thin coal seam. Journal Of China Coal Society. 2009; 34(6): 840-844. doi: 10.13225/j.cnki.jccs.2009.06.014